Correlations between variations in solar EUV and soft X-ray irradiance and photoelectron energy spectra observed on Mars and Earth

W. K. Peterson,[1] D. A. Brain,[1] D. L. Mitchell,[2] S. M. Bailey,[3] and P. C. Chamberlin[4]

Received 24 July 2013; revised 18 September 2013; accepted 20 October 2013; published 12 November 2013.

[1] Solar extreme ultraviolet (EUV; 10–120 nm) and soft X-ray (XUV; 0–10 nm) radiation are major heat sources for the Mars thermosphere as well as the primary source of ionization that creates the ionosphere. In investigations of Mars thermospheric chemistry and dynamics, solar irradiance models are used to account for variations in this radiation. Because of limited proxies, irradiance models do a poor job of tracking the significant variations in irradiance intensity in the EUV and XUV ranges over solar rotation time scales when the Mars-Sun-Earth angle is large. Recent results from Earth observations show that variations in photoelectron energy spectra are useful monitors of EUV and XUV irradiance variability. Here we investigate photoelectron energy spectra observed by the Mars Global Surveyor (MGS) Electron Reflectometer (ER) and the FAST satellite during the interval in 2005 when Earth, Mars, and the Sun were aligned. The Earth photoelectron data in selected bands correlate well with calculations based on 1 nm resolution observations above 27 nm supplemented by broadband observations and a solar model in the 0–27 nm range. At Mars, we find that instrumental and orbital limitations to the identifications of photoelectron energy spectra in MGS/ER data preclude their use as a monitor of solar EUV and XUV variability. However, observations with higher temporal and energy resolution obtained at lower altitudes on Mars might allow the separation of the solar wind and ionospheric components of electron energy spectra so that they could be used as reliable monitors of variations in solar EUV and XUV irradiance than the time shifted, Earth-based, $F_{10.7}$ index currently used.

Citation: Peterson, W. K., D. A. Brain, D. L. Mitchell, S. M. Bailey, and P. C. Chamberlin (2013), Correlations between variations in solar EUV and soft X-ray irradiance and photoelectron energy spectra observed on Mars and Earth, *J. Geophys. Res. Space Physics*, *118*, 7338–7347, doi:10.1002/2013JA019251.

1. Introduction

[2] The primary energy source driving the inner planetary ionospheres and thermospheres of Venus, Earth, and Mars is solar extreme ultraviolet (EUV; 10–121 nm) and soft X-ray (XUV; 0–10 nm) radiation. Solar irradiance varies with solar longitude on solar cycle, solar rotation, and solar flare time scales. Uncertainties in EUV and XUV irradiance illuminating Venus, Earth, and Mars limit the usefulness of thermospheric codes in studies of their atmospheres [e.g., *Gronoff et al*., 2012]. To be useful in thermospheric and ionospheric codes, solar irradiance observations and/or models should have high spectral and temporal resolution [see, for example, *Richards et al*., 2006; *Peterson et al*., 2008; *Qian et al*., 2010, and *Lollo et al*., 2012] and either use proxies taken within a narrow range of solar longitudes facing the planet of interest or provide a correction due to solar center to limb variations [*Qian et al*., 2010]. Almost all solar irradiance observations are made at the Earth and have both observational biases and spectral and temporal limitations [e.g., *Chamberlin et al*., 2007, 2008; *Peterson et al*., 2012]. Most solar irradiance data are available on the Web site http://lasp.colorado.edu/lisird/. When used at Mars, solar proxies driving these models are shifted in time to account for the different range of solar longitudes illuminating Mars [e.g., *Fox and Yeager*, 2006].

[3] *Peterson et al*. [2009, 2012] have demonstrated that daily averaged photoelectron energy spectra obtained from the FAST satellite [*Carlson et al*., 2001] at Earth have observable spectral variations in response to variations in solar EUV and XUV variations. They have compared observed and modeled daily averaged photoelectron energy spectra and have shown that the disagreement between observed and modeled photoelectron energy power in five selected energy bands is on the order of 30% over solar rotation time scales. This was done using models of solar

[1]LASP, University of Colorado, Boulder, Colorado, USA.
[2]SSL, University of California, Berkeley, California, USA.
[3]Baradley School of Engineering, Virginia Polytechnic Institute and State University, Blacksburg, Virginia, USA.
[4]Solar Physics Laboratory, NASA Goddard Space Flight Center, Greenbelt, Maryland, USA.

Corresponding author: W. K. Peterson, LASP, University of Colorado, Boulder, CO 80303, USA. (bill.peterson@lasp.colorado.edu)

2169-9380/13/10.1002/2013JA019251

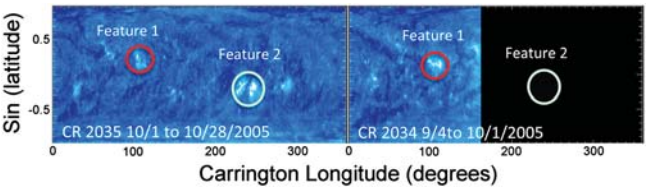

Figure 1. Data from the SOHO 17.1 nm imager for two Carrington rotations. Data are presented as a function of the sine of solar latitude and Carrington longitude. Note that in this format time goes from right to left. SOHO data were not available before 15 September as indicated by the lack of data in Carrington rotation 2034 from longitudes 360–160.

irradiance variations in the 0–50 nm range derived from spectrally limited and temporally sparse Thermosphere, Ionosphere, Mesosphere, Energetics, and Dynamics/Solar Extreme Ultraviolet Experiment [*Woods et al*., 2005] observations.

[4] Because Earth-based observations are available and directly relevant, the uncertainties in incident EUV and XUV irradiance at Mars are comparable to those at Earth during periods of alignment when the Mars-Sun-Earth angle is small (i.e., less than ~30°). At other times there are few, if any, solar irradiance observations at Mars. Significant additional uncertainty in the solar irradiance at Mars is introduced because the standard Earth-derived proxies for solar irradiance models have to be time shifted to account for the rotation of a solar feature seen on Earth to be seen on Mars. See, for example, *Mitchell et al*. [2001], *Jain and Bhardwaj* [2011], and *Gronoff et al*. [2012]. During periods of nonalignment the uncertainties in EUV and XUV irradiance energy input to Mars are so large that it is reasonable to consider the possibility of using variations in photoelectron intensity on Mars to monitor variations in incident solar EUV and XUV fluxes. The purpose of this paper is to investigate this possibility. This paper presents comparisons of variations in electron energy spectra observations from the Mars Global Surveyor (MGS) Electron Reflectometer (ER) [*Acuña et al*., 1992, 2001; *Mitchell et al*., 2001; *Brain et al*., 2007] with those observed in the photoelectron electron energy spectra at Earth detected by FAST. Suitable MGS/ER data are available from 1997 to 2006; suitable FAST data are available from 1997 to 2009. The comparisons are made during the interval in 2005 when Earth, Mars, and the Sun were aligned.

[5] The paper is organized as follows. We first describe the relative positions of active regions on the Sun with respect to Earth and Mars in late 2005. We then briefly review the technique developed by Peterson and his colleagues to relate variations in solar irradiance with variations in photoelectron energy in selected energy bands and apply this to data obtained from the FAST satellite at Earth during the interval of interest. This is followed by a discussion of how this technique has to be modified to accommodate differences in the plasma environment around Mars and features of electron observations made in this environment by the MGS/ER. We discuss the limitations of the MGS/ER Martian observations and conclude with a discussion on what electron observations might be used to monitor variations in solar EUV and XUV energy input to the Martian thermosphere and ionosphere.

2. Observations

2.1. Sun

[6] In the fall of 2005 the Sun, Mars, and Earth were nearly aligned, and there was recurring solar activity monitored by the Extreme Ultraviolet Imaging Telescope (EIT) on NASA's Solar and Heliophysics Observatory (SOHO). Figure 1 shows SOHO EIT Carrington maps from synoptic full-disk data from the iron line at 17.1 nm for Carrington rotations 2034 (4 September to 1 October 2005) and 2035 (1–28 October 2005). Time runs from right to left in Carrington rotation synoptic maps. See, for example, *Ulrich and Boyden* [2006] for information on how these synoptic maps are created. SOHO data were not available before 15 September. Two features in the solar data are indicated. The first was seen nearest the center of the solar disk on 24 September and again on 20 October. The second was seen nearest the center of the solar disk on 12 October.

[7] Figure 2 presents more information about the spectral, spatial, and temporal evolution of the irradiance seen at Earth and Mars for the period from 1 September to 16 October 2005. The green line in Figure 2a indicates the Earth-Sun-Mars angle as a function of time. Figure 2a also shows the angles of the two solar features identified in Figure 1 as seen from Earth and Mars. Feature 1 is shown in solid lines; feature 2 is shown with dotted lines. Red lines indicate Mars; black lines indicate Earth. Figures 2b–2d present the $F_{10.7}$, MgII, and GOES X-ray proxies of solar activity as measured on the Earth [see, for example, *Chamberlin et al*., 2008]. The dotted vertical lines appear for 13 and 24 September and 12 October, the days features identified in Figure 1 are closest to the center of the Sun's disk observed from Earth. Figure 2a shows that variations in solar irradiance during this interval associated with activity at the features seen near the center of the Sun's disk were seen simultaneously at both Earth and Mars. A detailed look at the observations from which the Carrington displays shown in Figure 1 were constructed shows that solar activity was not limited to the two regions identified and that some of the activity was near the solar limbs, which would not be visible simultaneously on Earth and Mars.

[8] Figures 2b–2d illustrate the diverse variations in solar irradiance proxies obtained at Earth used to drive various solar irradiance models. Until the launch of NASA's Solar Dynamics Observatory spacecraft in 2010 [*Woods et al*., 2010] variations in solar irradiance were sparsely sampled as a function of time and wavelength. Chamberlin and his colleagues have used proxies of solar irradiance variations and solar irradiance observations to construct a model of solar irradiance at high temporal (60 s) and spectral (1 nm) resolution. This Flare Irradiance Spectral Model (FISM, *Chamberlin et al*. [2007, 2008]) has been shown to agree well with observed variations in photoelectron intensity seen at solar flare, solar rotation, and solar cycle time scales [*Peterson et al*., 2008, 2009, 2012]. In the next subsection we compare and contrast photoelectron observations with those calculated using the FISM model for the interval shown in Figures 1 and 2.

2.2. Earth

[9] *Peterson et al*. [2008, 2009, 2012] have shown how to assemble and compare observed and modeled photoelectron

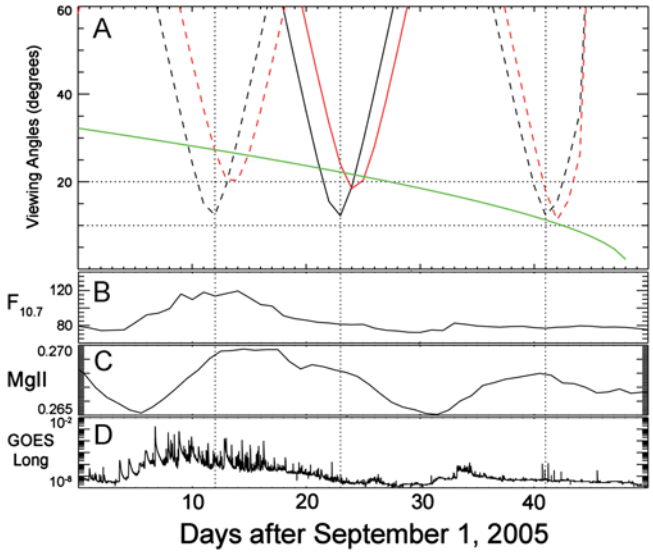

Figure 2. Further details of solar activity as seen on Earth and Mars. (a) Viewing angles: The green line shows the Earth-Sun-Mars angle in degrees as a function of time. The other lines indicate the angles of the two solar features identified in Figure 1 as seen from Earth and Mars. Red lines indicate Mars; black lines indicate Earth. Feature 1 is shown in solid lines; feature 2 is shown with dotted lines. The dotted vertical lines appear for 13 and 24 September and 12 October, the days the features identified in Figure 1 are closest to the center of the Sun's disk observed from Earth. Note that the time interval shown in Figure 2 is shorter than that shown in Figure 1. (b) Solar $F_{10.7}$ index values in solar flux units (10^{-22} W m^{-2} Hz^{-1}). (c) The nondimensional solar magnesium II index (core-to-wing ratio at 280 nm) values. (d) GOES long values: Intensity of the 0.7 nm X-ray intensity observed by one of NOAA's GOES satellites. The logarithmic scale covers the range from 10^{-8} to 10^{-2} W/m^2.

energy distributions and relate them to variations in solar irradiance over various time scales. The observations are all from an electron spectrometer on the FAST spacecraft [*Carlson et al*., 2001]. The data used were obtained at latitudes below the auroral zone and at altitudes above 1500 km. Data processing included correction for the spacecraft potential, removal of the background signal, and creation of daily averages to improve the signal-to-noise ratio at the highest energies. For comparison with observations, *Peterson et al*. [2012] used two photoelectron production codes driven by five different solar irradiance models to investigate uncertainties in solar energy input to the thermosphere on solar rotation time scales.

[10] Figure 3 presents and compares observed and modeled photoelectron spectra at Earth for the interval shown in Figures 1 and 2 using the techniques and some of the models described in *Peterson et al*. [2012]. Figure 3a shows the daily average observed escaping flux of photoelectrons as a function of energy from 10 eV to 1 keV encoded using the color bar on the right. Vertical black lines are drawn the same dates highlighted in Figures 1 and 2. Since most of the variation in photoelectron flux intensity is seen above about 30 eV, it is convenient to display photoelectron energy spectra as a function of equivalent wavelength. Equivalent wavelength is calculated from the Planck relation between energy and frequency assuming a constant 15 eV ionization potential as described by *Peterson et al*. [2008]. Figure 3b shows the observed daily averaged photoelectron power density in the same five equivalent wavelength bands used by *Peterson et al*. [2008, 2009, 2012] as a function of time. The power density in units of W/m^2 is encoded by the color bar on the right. Figure 3c shows the relative difference between the observations shown in Figure 3b and the average as a function of equivalent wavelength observed over the entire interval. The relative difference is encoded using the color bar on the right. Here relative difference = (observations − average)/average. If the observations were constant, the relative difference would be 0 and Figure 3c would be solid green. During two intervals, before about 16 September and centered on 14 October, relatively more intense photoelectrons were observed below ~10 nm (above about 100 eV) than on average. We note, and discuss further below, that the variations seen in the GOES X-ray fluxes in Figure 2d follow a similar pattern of intensity variation with time.

[11] Figure 3d presents calculated daily average photoelectron power density in the same five equivalent wavelength bands. The daily average is calculated from model calculations made at the times and locations of the observations. Here we use the FISM model solar irradiance spectrum and the Field Line Interhemispheric Plasma model (FLIP) [*Richards*, 2001, 2002, 2004, and references therein]. Figure 3e shows the relative difference between the observations and the photoelectron spectrum calculated using the FLIP/FISM model pair. Here relative difference = (observations − calculations)/observations. The difference is encoded using the color bar on the right. If the observations and calculations agreed at all times and equivalent wavelengths, Figure 3e would be solid green. On average the agreement between the observed and calculated fluxes is quite good especially above ~20 nm equivalent wavelength where solar rotational variability is less [*Peterson et al*., 2012]. We note, and discuss further below, that not all of the variations are completely captured by the FLIP/FISM model pair; nor do they follow variations in the solar $F_{10.7}$ index shown in Figure 3f.

2.3. Mars

[12] The limitations to FAST observations of photoelectron spectra at Earth are detector sensitivity and noise introduced by high-energy particles. The MGS/ER reflectometer is more sensitive than the FAST electron spectrometer [*Acuña et al*., 1992; *Carlson et al*., 2001]. The noise introduced in electron measurements by high-energy particles is significantly less at Mars. At Earth there are large regions where photoelectrons are well isolated from solar wind, auroral, and cusp electrons. The Mars magnetic field is not as strong and well organized as it is at Earth. In some regions of the sunlit hemisphere, the crustal magnetic field is strong enough that the MGS spacecraft (at ~400 km altitude) travels through closed field lines anchored in the crust and ionospheric photoelectrons dominate. In other regions, the crustal field is weak and the spacecraft travels through draped solar wind magnetic field lines, where both solar wind and ionospheric electrons can be present, depending on the minimum altitude sampled by the field line. The complex and time variable distribution of crustal magnetic cusps represent a third possibility. Consequently, the separation of solar wind and ionospheric photoelectrons at

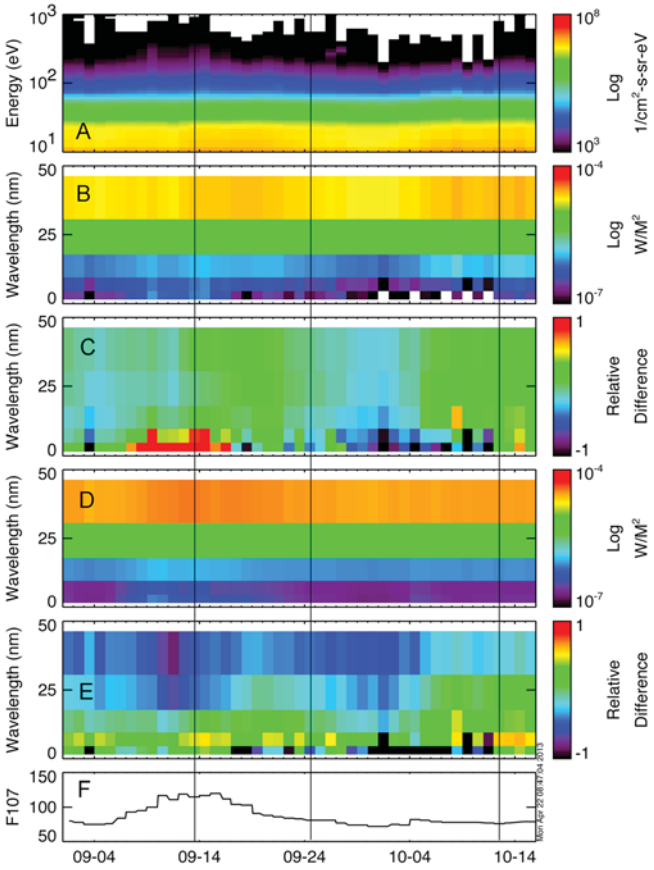

Figure 3. Observed and modeled terrestrial photoelectron energy spectra from 1 September to 16 October 2005. Vertical black lines are drawn for 13 and 24 September as well as 12 October. (a) Daily average of the observed photoelectron flux encoded using the color bar on the right as a function of energy. (b) Daily average of the observed photoelectron power density in five equivalent wavelength bands. The power density in units of W/m^2 is encoded by the color bar on the right. (c) Relative difference between the observations shown in Figure 3b and the average as a function of equivalent wavelength observed over the entire interval encoded using the color bar on the right. (d) Calculated daily average photoelectron power density in the same five equivalent wavelength bands used in Figure 3c. The power density is encoded using the color bar on the right. (e) Relative difference encoded using the color bar on the right using the observations seen in Figure 3b and the calculation seen in Figure 3d. (f) Daily solar $F_{10.7}$ index.

Mars is not as complete and depends on time and location. At Mars the presence of one or more features in the electron spectra is used to identify photoelectron spectra. These features are associated with HeII 30.4 nm emissions [*Frahm et al*., 2007], Auger electrons [*Mitchell et al*., 2000], and the sharp decrease in solar irradiance below ~16 nm [e.g., *Peterson et al*., 2012]. The identification of photoelectrons on Mars is now routinely used to identify boundaries between the Martian ionosphere and the shocked solar wind. See, for example, *Mitchell et al*. [2000, 2001], *Liemohn et al*. [2003], *Frahm et al*. [2006, 2007], *Brain et al*. [2007], and *Dubinin et al*. [2006, 2008].

[13] To provide a reliable monitor of variations in solar EUV and XUV irradiance, Martian electron spectra used must have a minimal solar wind electron component. Here we use details of the observed energy and angular distributions to attempt to identify electron distributions with minimal solar wind electron content. It is well known that for an energy-dependent range of angles around 90° pitch angle the signal to any electron detector is contaminated by blockage by and/or photoemissions from spacecraft surfaces [e.g., *Peterson et al*., 2009]. *Liemohn et al*. [2003] have developed a pitch angle dependent photoelectron production and transport code. Their analysis shows that the best model data comparisons are possible for field-aligned electrons. For this reason pitch angle resolved data from the MGS/ER are considered here. The electron reflectometer has 30 logarithmically spaced energy steps from 10 eV to 20 keV. The eight steps from 10 to 100 eV are all resolved in pitch angle. Pitch angle data from the remaining 22 steps are averaged over two adjacent energy steps, for a total of 19 pitch angle resolved energy bands. In the mapping orbit data considered here the radii of curvature of electrons for these 19 energy steps in the magnetic fields encountered are large compared to spacecraft dimensions. We exclude from the analysis data acquired in the 7 of the 16 angular sectors looking toward the spacecraft. To improve the signal-to-noise ratio at the highest energies we consider daily average Martian photoelectron fluxes.

[14] Figure 4 presents the pitch angle resolved electron energy spectra obtained on 20 September 2005 as a function time. Figures 4a–4e display pitch angle ranges 0–30°, 30–60°, 60–120°, 120–150°, and 150–180°, respectively, over the energy range from 11 eV to 1 keV. The flux intensity is encoded using the color bar on the right. A three-step process is used to obtain photoelectron spectra from MGS/ER data obtained from 14 September to 15 December 2005. The first step is to filter data based on location where they were acquired. We select spectra obtained only when the solar zenith angle at the satellite was less than 90°. To focus on photoelectrons produced deeper in the ionosphere and close to the sunlit satellite, we require that the magnetic declination (i.e., angle of the magnetic field from the local horizontal) was greater than 30° or less than −30°. For the data acquired on 20 September 2005 in the 0–30° pitch angle range 1080 spectra were selected for further processing. For the 30–60° range it was 1718; for the 60–120° range it was 1979; for the 120–150° range it was 1531; and for the 150–180° range it was 934. We corrected for the spacecraft potential using comparisons of observed energy spectra with those calculated using a modified GLOW code [*Solomon and Qian*, 2005, and references therein] that included CO_2 cross sections provided by Dr. Jane Fox and a neutral atmosphere provided by Dr. Ian Stewart. As expected we found that the correction for the spacecraft potential was less than a few volts.

[15] Next, for each day of data, we examined the ratios of electron fluxes at selected pairs of energy steps to identify electron data that have characteristic photoelectron flux energy distributions. Our filter uses the 19 energy steps for which pitch angle information is available. It is adapted from filter used by *Brain et al*. [2007] to identify photoelectron energy spectra using 30 energy step omnidirectional data. Figure 5 shows the 1080 electron energy spectra obtained in the 0–30° pitch angle range on 20 September 2005. One hundred six of these spectra, shown in orange, passed the shape filter based on ratios of fluxes at the energies indicated by the dotted vertical lines. The daily average of the 106

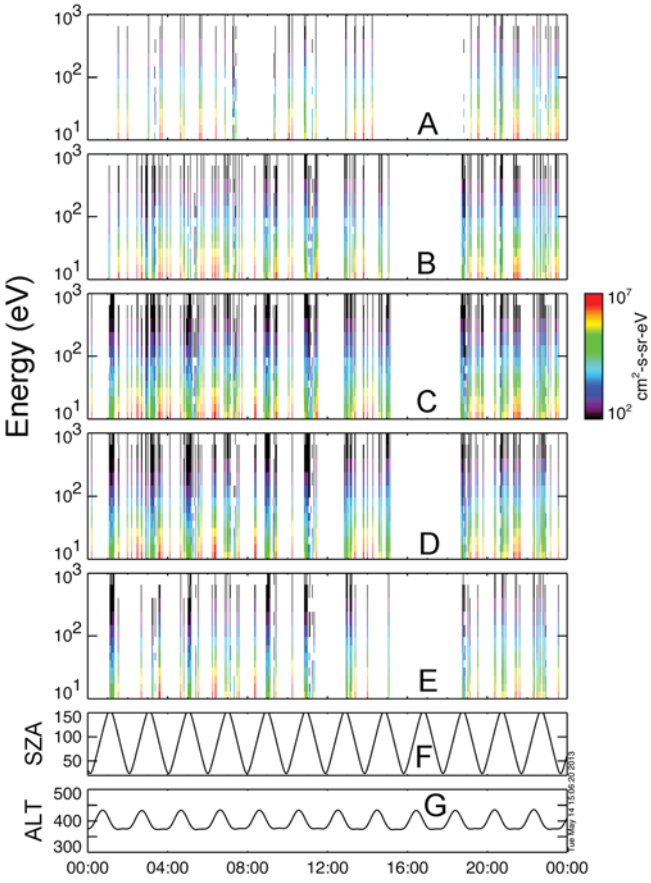

Figure 4. Pitch angle resolved energy spectra obtained on 20 September 2005 from the MGS/ER instrument. (a–e) Electron energy spectra as a function of time with the intensity encoded in units of $(cm^2\,s\,sr\,eV)^{-1}$ using the color bar on the right. Figures 4a–4e display pitch angle ranges 0–30°, 30–60°, 60–120°, 120–150°, and 150–180°, respectively, over the energy range from 10 eV to 1 keV. (f) The solar zenith angle in degrees at the location where the electron spectra were obtained. (g) The altitude in kilometers at the location where the electron spectra were obtained.

selected spectra in the 0–30° range is indicated by the green line. Data for the four other pitch angle ranges are also processed in this way.

[16] Examination of several days of data that pass the daily energy step filter showed that a small number of spectra with relatively high fluxes in the 20 eV range were passing the 19-energy-step photoelectron shape filter described above. These energy spectra represent a mixture of shocked solar wind and ionospheric photoelectrons. We therefore applied a third filter on the MGS/ER data to improve separation of photoelectron spectra and those mixed with shocked solar wind plasma. Figure 6 presents the 7353 electron spectra obtained from 14 September to 15 December that passed the daily shape filter for pitch angles between 0° and 30°. The third filter uses the distribution of flux intensity at 20 eV in 20 bins. It rejects spectra that are in intensity bins that contain at least 5% of the spectra with the highest flux at 20 eV. The fraction rejected depends on the shape of the intensity distribution. The flux level corresponding to the intensity bin selected is indicated by the horizontal blue line

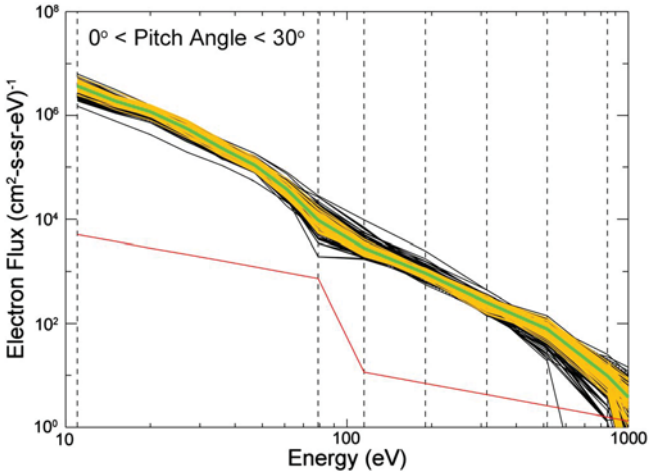

Figure 5. Partially filtered MGS/ER electron spectra for 20 September 2005. The 106 electron spectra passing the energy step filter are shown in orange. The average of these 106 spectra is shown as a solid green line. The solid red line shows the instrumental background (dominated by penetrating particles). See text.

in Figure 6. The 6603 spectra that have the flux intensity at 20 eV below the cutoff level are selected for further processing. The green spectra shown in Figure 6 is the average of the 6603 spectra passing the third filter. The same third filter is applied to data in the other four pitch angle ranges.

[17] To see what, if any, pitch angle variation there is in the photoelectron energy spectra selected using the process described above, we examined the scatter of flux values at selected energies. Figure 7 shows scatterplots of the flux intensity at 30 eV as a function of altitude. The solid horizontal lines show the average flux. The pitch angle ranges are color coded as indicated. Data for the 0–30° range were plotted last and over plots of data from other pitch angle ranges. Visual inspection shows that the scatter of the data in the 0–30° range

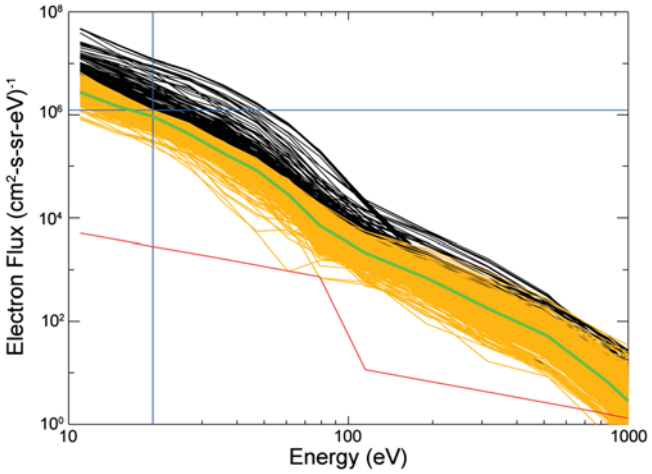

Figure 6. The 7353 electron spectra in the 0° to 30° range passing the daily shape filter between 14 September and 15 December 2005. A third filter, described in the text, selects 6603 for further processing. The selected spectra are shown in orange. The average of the selected spectra is shown as a green line. The solid red line is the detection threshold.

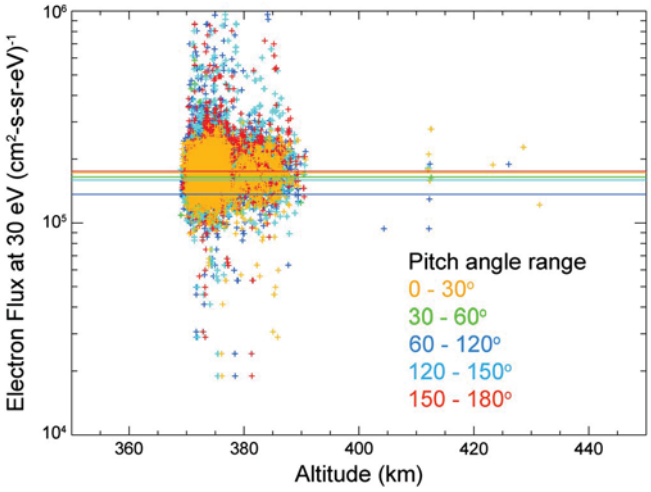

Figure 7. Scatterplots of the flux intensity at 30 eV as a function of altitude for the color-coded pitch angle ranges indicated. The color-coded solid horizontal lines show the average flux for the indicated pitch angle ranges.

is lower. The observations reported here are made in the altitude range from ~370 to ~430 km, well above the region of peak photoelectron production. At this altitude there are two possible geometries for observing photoelectrons: (1) on field lines with both feet in the ionosphere below (i.e., the trapped geometry) and (2) on field lines with only one foot in the ionosphere (i.e., the open geometry). In the trapped geometry photoelectrons are observed at both 0° and 180° pitch angles, i.e., from both the "near" and "far" feet of the field line. In this geometry the flux of photoelectrons reflected back from the opposite feet of the field lines is small and decreasing above ~20 eV [*Richards and Peterson*, 2008]. Since the focus of this paper is on variations in solar illumination, contributions to the flux from reflections are not relevant because the reflected component does not vary strongly with energy.

[18] We note that auroral acceleration has been observed associated with the closed magnetic field geometry [*Bertaux et al.*, 2005]. These processes modify the photoelectron spectra significantly; they are rejected by our filters. There are many possible reasons for the large scatter of data points seen in Figure 7. The most probable one is that the procedure outlined above to select photoelectron spectra is not perfect. Another reason for relatively more scatter at pitch angles between 30° and 150° is that the relatively large cross section for electron scattering on CO_2 are magnified by variations in effective path length at larger pitch angles. For these reasons the rest of this paper focuses on the Martian 0–30° pitch angle data.

[19] Figure 8 presents the filtered MGS/ER data from 14 September to October. Figure 8a shows all photoelectron energy spectra in the 0–30° pitch angle range. The continuity in time of the data in Figure 8a is an artifact of the display software. A varying number of photoelectron spectra were obtained per day as shown in Figure 8d. Figure 8b shows the daily average photoelectron intensity in the same five energy bins used in Figure 3 as a function of equivalent wavelength. Figure 8c shows the relative difference between the observations shown in Figure 8b and the average as a function of equivalent wavelength observed over the entire interval. The relative difference = (observations – average)/average. If the observations were constant, the relative difference would be 0 and Figure 8c would be solid green.

[20] Figure 8 shows some, but not all, of the same temporal and spectral variations of photoelectron intensity seen in Figure 3c. The data for 5 October appear to be significantly more intense than those obtained on the adjacent days. Examination shows that nine photoelectron spectra in the 0–30° pitch angle range passed our filter process, while over 150 were available on the adjacent days.

3. Comparison of Photoelectron Spectra From Earth and Mars

[21] Figures 3 and 8 illustrate the similarities and differences between variations seen at Earth and Mars in photoelectron

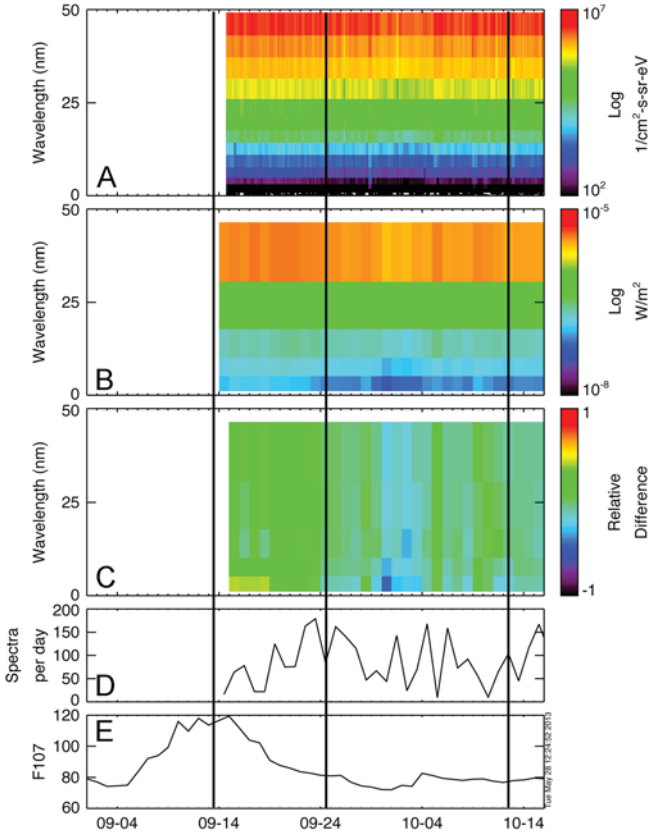

Figure 8. Observed Martian daily photoelectron energy spectra from 15 September to 16 October 2005 for the time range shown in Figure 3. No daily average MGS/ER in the 0–30° pitch angle range are available from 1 to14 September. Vertical black lines are drawn for 13 and 24 September as well as 12 October. (a) All observed photoelectron flux observations encoded using the color bar on the right as a function of energy. (b) Daily average of the observed photoelectron power density in five equivalent wavelength bands. The power density in units of W/m^2 is encoded by the color bar on the right. (c) Relative difference between the observations shown in Figure 8b and the average as a function of equivalent wavelength observed over the entire interval encoded using the color bar on the right. (d) Number of photoelectron spectra included in the daily average. (e) Daily solar $F_{10.7}$ index.

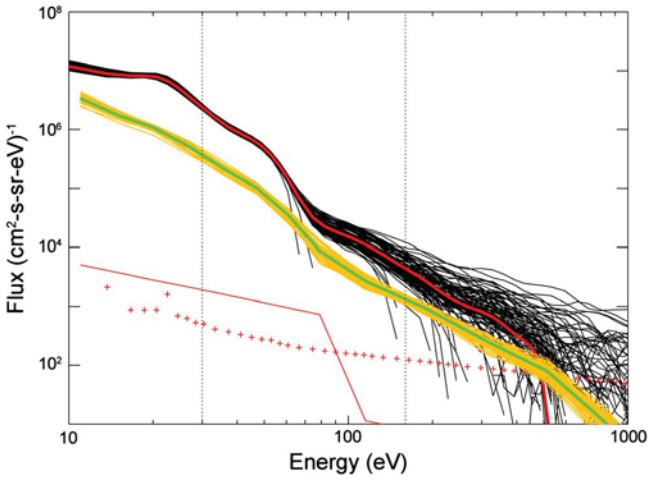

Figure 9. Photoelectron spectra acquired on the FAST satellite at Earth (black) and on the MGS satellite at Mars in the pitch angle range 0–30° on 20 September 2005. The average Earth spectrum is shown in red, and the average Mars spectrum is shown in green. . The red plus symbols show the 1 standard deviation uncertainty in the average Earth flux value based on the number of counts detected. The solid red line at the bottom is the instrument background of the Mars electron detector. The vertical dotted lines are at 30 and 110 eV as they are in Figure 6.

intensity during an interval when the Earth-Mars-Sun angle is small and there is modest solar activity. Figure 9 presents the 106 Mars MGS/ER filtered photoelectron energy spectra (orange) and the 96 Earth FAST photoelectron energy spectra (black) acquired on 20 September 2005. The daily average FAST spectrum is indicated in red and that for Mars is in green. The red plus symbols in Figure 9 show the 1 standard deviation uncertainty in the average Earth flux value based on the number of counts detected. At energies above ~500 eV the daily average Earth photoelectron fluxes are below the instrumental detection threshold. The solid red line at the bottom is the instrument background of the Mars electron detector. The observed Martian photoelectron fluxes are well above background over the energy range displayed.

[22] There is a remarkable difference in the scatter in the two data sets in Figure 9 at energies above about 100 eV. This difference arises because the MGS/ER has two selectable entrance apertures, which cover the same field of view but differ in their transmission by a factor of 43.5 [*Acuña et al*., 1992; *Mitchell et al*., 2001]. The FAST electron spectrometer has a constant geometric factor, which results in relatively fewer counts at the highest energies. For this reason *Peterson et al*. [2009, 2012] use daily average spectra to improve the signal-to-noise ratio above 25 eV where the variations in solar EUV and XUV intensity below 30 nm produce the most variability in photoelectron energy spectra.

[23] The shape of Mars photoelectron energy spectra reported here depends on details of production and transport processes and on imperfections in the photoelectron filtering process described above, which can lead to some solar wind electron contamination in the selected spectra. The shape of Earth photoelectron energy spectra depends on the correction for background and counting statistics. The relative magnitudes of photoelectron fluxes observed on Earth and Mars also depend on solar irradiance. Solar irradiance scales as $1/R^2$, where R is the distance from the Sun. On 20 September the irradiance at Earth was 1.97 times more intense than at Mars. The ratio of photoelectron intensities as a function of energy shown in Figure 9 is, however, not uniform with energy. The ratio is about 3 at 300 eV and increases nonuniformly to about 7 at 20 eV. Some of this variation can be attributed to instrumental uncertainties in the FAST data above about 100 eV. However, differences in production and transport processes associated with dominant nitrogen-oxygen atmosphere at Earth and dominant CO_2 atmosphere at Mars must also be considered. *Doering et al*. [1976] and *Lee et al*.

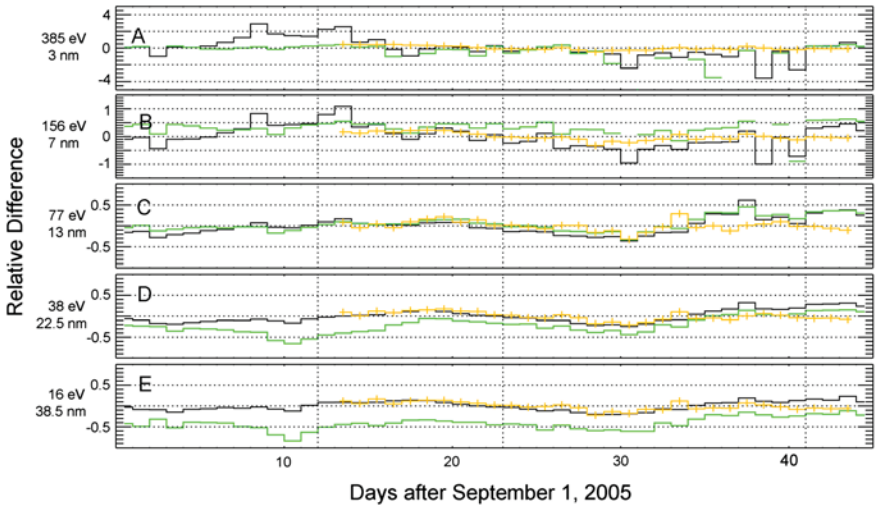

Figure 10. Relative difference between photoelectrons in five energy bands observed at Earth (black) and Mars (orange) and calculated for Earth (green) for 45 days starting on 1 September 2005. The center energy and equivalent wavelength are shown on the left for each band. The relative difference is the observed/calculated value − average divided by the average. Note that the scale of relative differences is (a) ±4, (b) ±1.5, and (c–e) ±0.5. The dotted vertical lines appear for 13 and 24 September and 12 October, the days the features identified in Figure 1 are closest to the center of the Sun's disk observed from Earth.

Table 1. Correlation Coefficients Between Photoelectron Observations, and Calculations and EUV/XUV Proxies for the Interval 1 September to 15 October 2005 for Five Selected Energy Bands

Band Center (nm)	Band Center (eV)	Earth-Mars	Earth-FLIP/FISM Calculation	Earth-$F_{10.7}$	Earth-GOES Max	Earth-MgII index
3	385	0.43	0.65	0.64	0.32	−0.48
7	156	0.57	0.40	0.69	0.24	−0.65
13	77	0.20	0.93	0.17	−0.03	−0.45
22.5	38	0.34	0.85	−0.01	−0.15	−0.42
38.5	16	0.48	0.76	0.26	−0.06	−0.60

[1980a, 1980b] have documented the variation in the shape of Earth's photoelectron energy spectrum as a function of altitude for solar minimum conditions. Spectral peaks in the energy distribution from photoionization of the dominant species by intense HeII at 30.4 nm can be resolved in the production region below about 200 km but are significantly broadened by scattering process when they are observed at higher altitudes at Earth and Mars [*Doering et al*., 1976; *Frahm et al*., 2007]. The Doering and Lee papers also show relatively small (compared to the differences between Mars and Earth spectra seen in Figure 9) changes in the slope of the photoelectron energy spectrum between 20 and the 100 eV upper limit of the sensitivity of the Atmosphere Explorer photoelectron spectrometers.

[24] The focus of this paper is not on the energy dependence of photoelectron spectra in different atmospheres. Rather, it is on the relationships between variations in photoelectron energy fluxes in limited energy ranges to variations in solar EUV and XUV irradiance as indicated in spectrogram format in Figures 3c and 8c. Figure 10 presents the relative difference between the observed and average Earth (black) and Mars (orange) photoelectron power in the five equivalent wavelength bands used by *Peterson et al*. [2009, 2012]. The green lines shown in Figure 10 are from the calculations based on the photoelectron energy spectra calculated using the FLIP model with solar irradiance input from the FISM model presented above in Figure 3e. Visual inspection of Figure 10 shows intervals of several days where the relative differences of photoelectron intensity at Earth and Mars have similar variations over a few days. For example, the relative differences in the highest energy (3 nm, Figure 10a) Earth and Mars band from 19 to 29 September are similar. Also, the relative differences in Earth observations closely follow calculations based on the FLIP/FISM model pair (green lines) in Figures 10c–10e.

[25] The correlation between the variations in photoelectron intensity in selected bands measured at Earth and Mars shown in Figure 10 can be quantified by calculating correlation coefficients. Data from both Earth and Mars are available for 31 of the 45 days shown in Figure 10. Table 1 presents the correlations coefficients between observations at Earth and various quantities including observations at Mars. Also shown in Table 1 are the correlations between variations in the intensity of photoelectrons at Earth in selected energy bands and the $F_{10.7}$, GOES X-ray, and MgII index proxies for solar EUV and XUV irradiance variability. Because continuous Earth-based data are available, these correlations are for the full 45 day interval between 1 September and 15 October.

[26] The correlations between photoelectron observations at Earth and Mars shown in the third column of Table 1 are weak to moderate. That is, the correlation coefficients are in the range from 0.2 to 0.6. They vary from a maximum of 0.57 in the 7 nm band to 0.20 in the 13 nm band. The correlations between photoelectron observations at Earth and those calculated using the FLIP/FISM model pair are, however, moderate to very strong, varying from a low of 0.4 in the 7 nm band to a high of 0.93 in the 13 nm band. The last three columns of Table 1 show weak to moderate (0.01 to 0.69) correlations between observations at Earth and three of the most common Earth-based proxies for solar EUV and XUV variations.

[27] The weak to moderate correlation between photoelectron observations at Earth and the $F_{10.7}$ and MgII index, and the daily maximum power in the 0.7 nm X-ray flux measured on the National Oceanic and Atmospheric Administration's (NOAA's) GOES satellites is well known and documented. See, for example, *Chamberlin et al*. [2007, 2008]. The FISM irradiance model [*Chamberlin et al*., 2007, 2008] uses a variable mix of observations and indices to provide more realistic solar irradiance spectra. *Peterson et al*. [2008, 2009, 2012] have shown that the observed and FLIP/FISM modeled photoelectron energy spectra generally agree to within model and observational uncertainties. *Peterson et al*. [2012] have shown that on solar rotation time scales about 30% of the observed variability in the photoelectron flux intensity is not captured by the FLIP/FISM or other code/irradiance model pairs investigated. The moderate to strong correlations shown in the fourth column of Table 1 are consistent with the results presented in *Peterson et al*. [2012].

4. Discussion

[28] Because the photochemistry of the Martian and Earth ionospheres are not that dissimilar [e.g., *Schunk and Nagy*, 1980], we can reasonably expect that variations in EUV and XUV irradiance at Mars cause similar variations in photoelectron intensity at Earth. Furthermore, the variations in photoelectron intensity at Mars should be correlated to those at Earth when the same side of the solar disk illuminates both planets. We have analyzed data for a time interval when the Earth-Sun-Mars angle is less than 30° and there is moderate activity on the Sun. Table 1 shows that variations in solar irradiance proxies and calculations using the FLIP/FISM model pair are moderately to strongly correlated with variations in observed photoelectron energy spectra in various energy bands. In contrast, Figure 10 and Table 1 demonstrate that there is weak to moderate correlation between variations in photoelectron intensity in selected energy bands at Earth detected on the FAST spacecraft and intensity variations in the photoelectron energy spectra derived from MGS/ER observations at Mars. This level of correlation means that variations of solar EUV irradiance incident on Mars cannot be reliably monitored by the MGS/ER observations presented above.

[29] At Mars identification of photoelectron spectra is made by confirming the presence of one or more features in the electron spectra associated with HeII 30.4 nm emissions, Auger electrons, and the sharp decrease in solar irradiance below ~16 nm. As shown in Figures 5 and 6, the filter we developed to select energy spectra dominated by photoelectrons

focuses on pitch angle resolved features associated with the HeII 30.4 nm emissions and the sharp decrease in solar irradiance below ~16 nm. Figures 5 and 6 show that electron energy spectra without the two features are easily identified. Because solar wind electrons can penetrate quite deeply into the ionosphere, Martian electron energy spectra with the two pitch angle resolved features could also include solar wind electrons. We note that the MGS/ER data presented here were acquired at altitudes between 370 and 440 km.

[30] The analysis and modeling work of *Frahm et al*. [2007], *Liemohn et al*. [2003], and others show that identifying photoelectron spectra in electron energy spectra obtained at Mars depends strongly on the altitude of data acquisition, the energy resolution of the detector, and the availability of pitch angle resolved energy spectra. *Frahm et al*. [2007] used photoelectron energy spectra obtained over a larger altitude range (250–10,000 km) from Mars Express (MEX). They have shown that, except at the lowest altitudes sampled, photoelectron energy spectra are not detected on every orbit. *Liemohn et al*. [2003] have developed a pitch angle dependent photoelectron production and transport code. They have identified regions of closed magnetic fields in the MGS/ER data and shown that MGS/ER electron energy and pitch angle observations agreed well with the calculations, considering the uncertainties in the Mars neutral atmosphere and solar irradiance. Their analysis also shows that the most sensitive model/data comparisons are possible when considering nearly magnetic field-aligned observations.

[31] We conclude that it is not possible to adequately separate photoelectrons and solar wind electrons in the electron spectra obtained by MGS/ER to be able to use them as a monitor of solar variability. The data do not have enough pitch angle resolved energy resolution and are not obtained at low enough altitudes. The MGS/ER data have two pitch angle resolved energy steps in the 20–30 eV region specific to the HeII 30.4 nm emissions and one pitch angle resolved energy step in the 60–70 eV region specific to the sharp dropoff in solar irradiance below 16 nm. The filters we have discussed above are not ideal because they have necessarily had to include energy steps outside of the optimal ranges and are obtained well above 250 km where *Frahm et al*. [2007] have found distinct HeII 30.4 nm features in MEX electron spectra on almost every orbit. The Mars electron data passing through our filters thus contain an unknown and variable fraction of solar wind electrons, which is reflected in the weak to moderate correlation with Earth observations shown in Table 1.

5. Conclusion

[32] At Earth photoelectron intensity in selected bands correlates well with calculations based on the FISM model, which is based on observations supplemented by a solar model in the 0–27 nm range. We find that limitations to the identifications of photoelectron energy spectra in MGS/ER data preclude their use as a more reliable monitor of solar EUV and XUV variability. However, observations obtained at lower altitudes, closer to the peak photoelectron production region, might allow the separation of the solar wind and ionospheric components of electron energy spectra so that they could be used as a more reliable model for variations in solar EUV and XUV irradiance than the time-shifted, Earth-based, $F_{10.7}$ index currently used. Such higher energy resolution pitch angle resolved observations below 250 km will soon be available on NASA's Mars Atmosphere and Volatile Evolution Mission (MAVEN, http://lasp.colorado.edu/home/maven/) to be launched in late 2013. MAVEN will also carry a solar EUV irradiance monitor providing a direct measure of the solar input in order to validate this relationship. The lack of a magnetometer precludes use of the technique described here for electrons detected on the Mars Express spacecraft [*Frahm et al*., 2007].

[33] **Acknowledgments.** We thank Ian Stewart, Jane Fox, Jim McFadden, and Phil Richards for data, models, and discussions. We thank the SOHO EIT team for images used in Figure 1. The GOES X-ray observations and indices in Figure 2 are from the NOAA SPIDR web site. We thank one of the reviewers for his/her constructive comments. W.K.P. was supported by NASA Grant NNX12AD25G.

[34] Philippa Browning thanks the reviewers for their assistance in evaluating this paper.

References

Acuña, M. H., et al. (1992), Mars Observer magnetic fields investigation, *J. Geophys. Res.*, *97*, 7799–7814.

Acuña, M. H., et al. (2001), Magnetic field of Mars: Summary of results from the aerobraking and mapping orbits, *J. Geophys. Res.*, *106*(E10), 23,403–23,417, doi:10.1029/2000JE001404.

Bertaux, J.-L., F. Leblanc, O. Witasse, E. Quemerais, J. Lilensten, S. A. Stern, B. Sandel, and O. Korablev (2005), Discovery of an aurora on Mars, *Nature*, *435*, 790–794, doi:10.1038/nature03603.

Brain, D. A., R. J. Lillis, D. L. Mitchell, J. S. Halekas, and R. P. Lin (2007), Electron pitch angle distributions as indicators of magnetic field topology near Mars, *J. Geophys. Res.*, *112*, A09201, doi:10.1029/2007JA012435.

Carlson, C. W., J. P. McFadden, P. Turin, D. W. Curtis, and A. Magoncelli (2001), The electron and ion plasma experiment for FAST, *Space Sci. Rev.*, *98*, 33.

Chamberlin, P. C., T. N. Woods, and F. G. Eparvier (2007), Flare Irradiance Spectral Model (FISM): Daily component algorithms and results, *Space Weather*, *5*, S07005, doi:10.1029/2007SW000316.

Chamberlin, P. C., T. N. Woods, and F. G. Eparvier (2008), Flare Irradiance Spectral Model (FISM): Flare component algorithms and results, *Space Weather*, *6*, S05001, doi:10.1029/2007SW000372.

Doering, J. P., W. K. Peterson, C. O. Bostrom, and T. A. Potemra (1976), High resolution daytime photoelectron energy spectra from AE-E, *Geophys. Res. Lett.*, *3*, 129–131.

Dubinin, E., M. Fränz, J. Woch, E. Roussos, S. Barabash, R. Lundin, J. D. Winningham, R. A. Frahm, and M. Acuña (2006), Plasma morphology at Mars. Aspera-3 observations, *Space Sci. Rev.*, *126*, 209–238, doi:10.1007/s11214-006-9039-4.

Dubinin, E., et al. (2008), Plasma environment of Mars as observed by simultaneous MEX-ASPERA-3 and MEX-MARSIS observations, *J. Geophys. Res.*, *113*, A10217, doi:10.1029/2008JA013355.

Fox, J. L., and K. E. Yeager (2006), Morphology of the near-terminator Martian ionosphere: A comparison of models and data, *J. Geophys. Res.*, *111*, A10309, doi:10.1029/2006JA011697.

Frahm, R. A., et al. (2006), Carbon dioxide photoelectron energy peaks at Mars, *Icarus*, *182*, 371–382, doi:10.1016/j.icarus.2006.01.014.

Frahm, R. A., et al. (2007), Locations of atmospheric photoelectron energy peaks within the Mars environment, *Space Sci. Rev.*, *126*, 389–402, doi:10.1007/s11214-006-9119-5.

Gronoff, G., C. Simon Wedlund, C. J. Mertens, and R. J. Lillis (2012), Computing uncertainties in ionosphere-airglow models: I. Electron flux and species production uncertainties for Mars, *J. Geophys. Res.*, *117*, A04306, doi:10.1029/2011JA016930.

Jain, S. K., and A. Bhardwaj (2011), Impact of solar EUV flux on CO Cameron band and CO_2+ UV doublet emissions in the dayglow of mars, *Planet. Space Sci.*, *63–64*, 110–122, doi:10.1016/j.pss.2011.08.010.

Lee, J. S., J. P. Doering, T. A. Potemra, and L. H. Brace (1980a), Measurements of the ambient photoelectron spectrum from Atmosphere Explorer: I. AE-E measurements below 300 km during solar minimum conditions, *Planet. Space Sci.*, *28*, 947–971.

Lee, J. S., J. P. Doering, T. A. Potemra, and L. H. Brace (1980b), Measurements of the ambient photoelectron spectrum from Atmosphere Explorer: II. AE-E measurements from 300 to 1000 km during solar minimum conditions, *Planet. Space Sci.*, *28*, 973–996.

Liemohn, M. W., D. L. Mitchell, A. F. Nagy, J. L. Fox, T. W. Reimer, and Y. Ma (2003), Comparisons of electron fluxes measured in the crustal fields at Mars by the MGS magnetometer/electron reflectometer instrument with a B field-dependent transport code, *J. Geophys. Res.*, *108*(E12), 5134, doi:10.1029/2003JE002158.

Lollo, A., P. Withers, K. Fallows, Z. Girazian, M. Matta, and P. C. Chamberlin (2012), Numerical simulations of the ionosphere of Mars during a solar flare, *J. Geophys. Res.*, *117*, A05314, doi:10.1029/2011JA017399.

Mitchell, D. L., R. P. Lin, H. Rème, D. H. Crider, P. A. Cloutier, J. E. P. Connerney, M. H. Acuña, and N. F. Ness (2000), Oxygen auger electrons observed in Mars' ionosphere, *Geophys. Res. Lett.*, *27*(13), 1871–1874, doi:10.1029/1999GL010754.

Mitchell, D. L., R. P. Lin, C. Mazelle, H. Rème, P. A. Cloutier, J. E. P. Connerney, M. H. Acuña, and N. F. Ness (2001), Probing Mars' crustal magnetic field and ionosphere with the MGS Electron Reflectometer, *J. Geophys. Res.*, *106*(E10), 23,419–23,427, doi:10.1029/2000JE001435.

Peterson, W. K., P. C. Chamberlin, T. N. Woods, and P. G. Richards (2008), Temporal and spectral variations of the photoelectron flux and solar irradiance during an X class solar flare, *Geophys. Res. Lett.*, *35*, L12102, doi:10.1029/2008GL033746.

Peterson, W. K., E. N. Stavros, P. G. Richards, P. C. Chamberlin, T. N. Woods, S. M. Bailey, and S. C. Solomon (2009), Photoelectrons as a tool to evaluate spectral variations in solar EUV irradiance over solar cycle timescales, *J. Geophys. Res.*, *114*, A10304, doi:10.1029/2009JA014362.

Peterson, W. K., T. N. Woods, J. M. Fontenla, P. G. Richards, P. C. Chamberlin, S. C. Solomon, W. K. Tobiska, and H. P. Warren (2012), Solar EUV and XUV energy input to thermosphere on solar rotation time scales derived from photoelectron observations, *J. Geophys. Res.*, *117*, A05320, doi:10.1029/2011JA017382.

Qian, L., A. G. Burns, P. C. Chamberlin, and S. C. Solomon (2010), Flare location on the solar disk: Modeling the thermosphere and ionosphere response, *J. Geophys. Res.*, *115*, A09311, doi:10.1029/2009JA015225.

Richards, P. G. (2001), Seasonal and solar cycle variations of the ionospheric peak electron density: Comparison of measurement and models, *J. Geophys. Res.*, *106*, 12,803–12,819, doi:10.1029/2000JA000365.

Richards, P. G. (2002), Ion and neutral density variations during ionospheric storms in September 1974: Comparison of measurement and models, *J. Geophys. Res.*, *107*(A11), 1361, doi:10.1029/2002JA009278.

Richards, P. G. (2004), On the increases in nitric oxide density at midlatitudes during ionospheric storms, *J. Geophys. Res.*, *109*, A06304, doi:10.1029/2003JA010110.

Richards, P. G., and W. K. Peterson (2008), Measured and modeled backscatter of ionospheric photoelectron fluxes, *J. Geophys. Res.*, *113*, A08321, doi:10.1029/2008JA013092.

Richards, P. G., T. N. Woods, and W. K. Peterson (2006), HEUVAC: A new high resolution solar EUV proxy model, *Adv. Space Res.*, *37*, 315–322, doi:10.1016/j.asr.2005.06.031.

Schunk, R. W., and A. F. Nagy (1980), Ionospheres of the terrestrial planets, *Rev. Geophys.*, *18*, 813–852.

Solomon, S. C., and L. Qian (2005), Solar extreme-ultraviolet irradiance for general circulation models, *J. Geophys. Res.*, *110*, A10306, doi:10.1029/2005JA011160.

Ulrich, R. K., and J. E. Boyden (2006), Carrington Coordinates and Solar Maps, *Sol. Phys.*, *235*, 17–29, doi:10.1007/s11207-006-0041-5.

Woods, T. N., F. G. Eparvier, S. M. Bailey, P. C. Chamberlin, J. Lean, G. J. Rottman, S. C. Solomon, W. K. Tobiska, and D. L. Woodraska (2005), Solar EUV Experiment (SEE): Mission overview and first results, *J. Geophys. Res.*, *110*, A01312, doi:10.1029/2004JA010765.

Woods, T. N., et al. (2010), Extreme Ultraviolet Variability Experiment (EVE) on the Solar Dynamics Observatory (SDO): Overview of science objectives, instrument design, data products, and model developments, *Solar Phys.*, *3*, 115–143, doi:10.1007/s11207-009-9487-6.